HHS Public Access

Author manuscript

Exp Neurol. Author manuscript; available in PMC 2024 January 23.

Published in final edited form as:

Exp Neurol. 2022 January ; 347: 113892. doi:10.1016/j.expneurol.2021.113892.

Nonsteroidal anti-inflammatory drug (ketoprofen) delivery differentially impacts phrenic long-term facilitation in rats with motor neuron death induced by intrapleural CTB-SAP injections

Lauren F. Borkowski,

Amy N. Keilholz,

Catherine L. Smith,

Kaylie A. Canda,

Nicole L. Nichols*

Department of Biomedical Sciences, Dalton Cardiovascular Research Center, University of Missouri, Columbia, MO 65211, USA

Abstract

Intrapleural injections of cholera toxin B conjugated to saporin (CTB-SAP) selectively eliminates respiratory (e.g., phrenic) motor neurons, and mimics motor neuron death and respiratory deficits observed in rat models of neuromuscular diseases. Additionally, microglial density increases in the phrenic motor nucleus following CTB-SAP. This CTB-SAP rodent model allows us to study the impact of motor neuron death on the output of surviving phrenic motor neurons, and the underlying mechanisms that contribute to enhancing or constraining their output at 7 days (d) or 28d post-CTB-SAP injection. 7d CTB-SAP rats elicit enhanced phrenic long-term facilitation (pLTF) through the Gs-pathway (inflammation-resistant in naïve rats), while pLTF is elicited though the Gq-pathway (inflammation-sensitive in naïve rats) in control and 28d CTB-SAP rats. In 7d and 28d male CTB-SAP rats and controls, we evaluated the effect of cyclooxygenase-1/2 enzymes on pLTF by delivery of the nonsteroidal anti-inflammatory drug, ketoprofen (IP), and we hypothesized that pLTF would be unaffected by ketoprofen in 7d CTB-SAP rats, but pLTF would be enhanced in 28d CTB-SAP rats. In anesthetized, paralyzed and ventilated rats, pLTF was surprisingly attenuated in 7d CTB-SAP rats and enhanced in 28d CTB-SAP rats (both $p < 0.05$) following ketoprofen delivery. Additionally in CTB-SAP rats: 1) microglia were more amoeboid in the phrenic motor nucleus; and 2) cervical spinal inflammatory-associated factor expression (TNF-α, BDNF, and IL-10) was increased vs. controls in the absence of ketoprofen ($p < 0.05$). Following ketoprofen delivery, TNF-α and IL-10 expression was decreased back to control levels,

*Corresponding author at: Department of Biomedical Sciences, University of Missouri, 1600 E. Rollins St., Columbia, MO 65211, USA. nicholsn@missouri.edu (N.L. Nichols).

Author contributions

N.L.N. designed research; L.F.B, A.N.K., C.L.S., K.A.C., and N.L.N. performed experiments, analyzed data, and interpreted results of experiments; L.F.B. and N.L.N. prepared figures and drafted the manuscript; and L.F.B, A.N.K., C.L.S., K.A.C., and N.L.N. edited and approved the final manuscript. This work was supported by grants or scholarships from the National Institutes of Health (NIH) K99/R00 HL119606 (N.L. N.), the University of Missouri Spinal Cord Injury/Disease Research Program (N.L.N.), the University of Missouri College of Veterinary Medicine Committee on Research (N.L.N.), and the American Veterinary Medical Association / American Veterinary Medical Foundation (AVMA/AVMF) 2nd Opportunity Research Scholarship (K.A.C.).

Declarations of interest

None.

while BDNF expression was differentially affected over the course of motor neuron death in CTB-SAP rats. This study furthers our understanding of factors (e.g., cyclooxygenase-1/2-induced inflammation) that contribute to enhancing or constraining pLTF and its implications for breathing following respiratory motor neuron death.

Keywords

Respiratory plasticity; Phrenic motor neuron death; Inflammation; Spinal cord; Breathing; Microglia

1. Introduction

A variety of neuromuscular/neurodegenerative diseases (e.g., spinal muscular atrophy (SMA), and amyotrophic lateral sclerosis (ALS)) and injuries (e.g., spinal cord injury) result in respiratory motor neuron loss and diminished respiratory muscle output, and ultimately death by ventilatory failure (Boentert et al., 2017; Bourke et al., 2001; Lechtzin et al., 2002; Lyall et al., 2001; Nichols et al., 2013; Nogués et al., 2002; Wong et al., 2002). Additionally, these patients experience systemic inflammation that hinders the function of the neural networks responsible for breathing (Perry, 2010; Teeling and Perry, 2009). However, breathing is maintained until mechanisms of compensation begin to fail or respiratory motor neuron loss becomes too great. To specifically study the effects caused by respiratory motor neuron loss, we utilize intrapleural injections of cholera toxin B conjugated to saporin (CTB-SAP) to induce targeted respiratory motor neuron death (Borkowski and Nichols, 2020; Nichols et al., 2018; Nichols et al., 2015).

Intrapleurally injected CTB-SAP results in phrenic motor neuron loss [~40% survival in 7 day (d) CTB-SAP rats and ~ 25% survival in 28d CTB-SAP rats] and increased microglial density in the phrenic motor nucleus at 7d and 28d post-CTB-SAP treatment (Nichols et al., 2018; Nichols et al., 2015). Interestingly, eupnea is maintained despite respiratory motor neuron loss (Nichols et al., 2015). We speculate that the surviving respiratory neurons utilize mechanisms of plasticity, such as phrenic motor facilitation (pMF), to maintain eupnea. (Mitchell et al., 2001). Phrenic long-term facilitation (pLTF) is a form of pMF induced by acute intermittent hypoxia (AIH). In naïve rats, moderate AIH (35–55 mmHg PaO_2) elicits pLTF through Gq-dependent mechanisms via serotonin 2 receptors (5-HT2) in the phrenic motor nucleus (Bach and Mitchell, 1996; Baker-Herman et al., 2004; Devinney et al., 2015; Devinney et al., 2013; Hoffman et al., 2012). Conversely, severe AIH (i. e., 25–35 mmHg PaO_2) elicits enhanced pLTF through Gs-dependent mechanisms via A2A receptors (Agosto-Marlin and Mitchell, 2017; Devinney et al., 2013; Golder et al., 2008; Nichols et al., 2012). Interestingly, 7d CTB-SAP rats exhibit Gs-pathway dependent enhanced pLTF, while 28d CTB-SAP rats utilize the Gq-pathway for modest pLTF (Borkowski and Nichols, 2020; Borkowski et al., 2021; Nichols et al., 2018). However, it remains unknown if there are factors [e.g., inflammation through cyclooxygenase 1 and 2 (COX-1 and 2)] contributing to the differential magnitude of pLTF exhibited in CTB-SAP rats.

Since microglial density is increased in the phrenic motor nucleus of CTB-SAP rats, we speculate that inflammation is one factor that contributes to differential pLTF. Gq pathway-

induced pMF and moderate AIH-induced pLTF are nearly abolished by lipopolysaccharide (LPS; a toll-like receptor 4 agonist (Lu et al., 2008; Triantafilou and Triantafilou, 2002)) induced inflammation, but is restored with ketoprofen (nonsteroidal anti-inflammatory drug) administration (Agosto-Marlin et al., 2018; Hocker et al., 2017; Huxtable et al., 2011; Huxtable et al., 2015; Huxtable et al., 2013; Vinit et al., 2011). In contrast, Gs pathway-induced pMF and severe AIH-induced pLTF are unaffected by LPS-induced inflammation, indicating that the Gs pathway is inflammation-resistant (Agosto-Marlin and Mitchell, 2017). However, the impact of inflammation (e.g., COX-1/2 activation) on pLTF following CTB-SAP-induced respiratory motor neuron death has yet to be studied. Furthermore, it remains unknown if cells associated with inflammation such as microglia are activated in CTB-SAP rats, where activation is typically indicated by an amoeboid morphological microglial phenotype. When there is an insult to the CNS, microglia will proliferate, rapidly migrate to the injury site, transition from ramified to amoeboid state (Graeber, 2010; Kreutzberg, 1996), and produce and release inflammatory-associated molecules (Huston and Tracey, 2011). Currently, changes in cervical spinal inflammatory-associated marker expression following CTB-SAP-induced respiratory motor neuron death are unknown.

Here, we studied how COX-1/2 mediated inflammation impacts pLTF, and how microglial morphology in the phrenic motor nucleus and cervical spinal (C3–5) expression of inflammatory-associated markers are impacted in CTB-SAP treated rats. We hypothesized that pLTF would be unaffected by ketoprofen (nonsteroidal anti-inflammatory drug) in 7d CTB-SAP rats (Gs-pathway is inflammation resistant), but ketoprofen would enhance pLTF in 28d CTB-SAP rats (Gq-pathway is inflammation sensitive). Additionally, we hypothesized that microglia in the phrenic motor nucleus would have morphological characteristics that are consistent with an activated phenotype. Furthermore, we hypothesized that cervical spinal (C3–5) expression of inflammatory-associated markers would be increased in CTB-SAP rats, and that ketoprofen delivery would reduce expression back to control levels.

2. Methods

2.1. Animals

Experiments were conducted on adult (3–4 months old) male Sprague Dawley rats (Envigo Colony 208; Indianapolis, IN). Rats were housed in pairs and maintained under a 12:12 light:dark cycle. Animals had access to a standard commercial pelleted diet and water ad libitum. All procedures in this manuscript were approved by the Institutional Animal Care and Use Committee at the University of Missouri in accordance with National Institutes of Health Guide for the Care and Use of Laboratory Animals. The University of Missouri is an AAALAC-accredited institution that operates under Animal Welfare Assurance ID A3394–01.

2.2. Intrapleural injections

Rats received bilateral intrapleural injections (6 mm deep, fifth intercostal space) using a 50 μl Hamilton syringe and a custom needle (6 mm, 23 gauge, semi-blunt to prevent lung puncture) while under isoflurane anesthesia (1.5% in 100% oxygen as previously

described by Mantilla et al. (2009). Control rats were intrapleurally injected with cholera toxin B subunit (CTB; 20 μg dissolved in doubly distilled H_2O; Calbiochem; Billerica, MA) unconjugated to saporin (SAP; 25 μg dissolved in phosphate buffered saline (PBS); Advanced Targeting Systems; San Diego, CA) to enable comparisons for respiratory plasticity, microglial morphology, and cervical spinal inflammatory-associated marker expression. CTB conjugated to saporin (CTB-SAP; 25 μg dissolved in PBS; Advanced Targeting Systems; San Diego, CA) was intrapleurally injected to target respiratory motor neurons as described previously (Nichols et al., 2015, 2018; Borkowski and Nichols, 2020). CTB-SAP treated rats also received an additional 20 μg of CTB dissolved in double distilled H_2O (Calbiochem; Billerica, MA) in their administered intrapleural injections. Rats were then monitored to ensure respiration was not compromised following intrapleural injections, and were housed for 7 or 28 days before the below surgical preparation and neurophysiological experiments were performed.

2.3. Surgical preparation for in vivo neurophysiological experiments

Experimental procedures were performed as described previously (e. g., Hoffman et al., 2012; Nichols et al., 2018). Briefly, rats were isoflurane anesthetized, tracheotomized, and pump ventilated (Small Animal SAR-1000 Ventilator; CWE, Ardmore, PA, USA; tidal volume ~ 2.5 ml, frequency ~ 70–80 breaths per minute). Rats remained under iso-flurane anesthesia (3.5% in 50% O_2, balance N_2) throughout surgical procedures before being converted to urethane anesthesia over 15–20 min (1.85 g kg^{-1}, *i.v.*) while isoflurane was slowly withdrawn. Once completely converted to urethane anesthesia, rats were then paralyzed for neuromuscular blockade using pancuronium bromide (2.5 mg kg^{-1}, i.v.). Rats were given a 1:2:0.13 mixture of 6% Hetastarch (in 0.9% sodium chloride), lactated Ringer's solution, and 8.4% sodium bicarbonate via continuous intravenous infusion (1.5–6 ml kg^{-1} h^{-1}) to maintain body fluid and acid-base balance. Lack of the pressor responses or obvious respiratory neural responses to a toe pinch with a hemostat was used to confirm the adequacy of anesthesia before and immediately after surgical and neurophysiological protocols were complete. Body temperature was maintained (37 ± 1 °C) with a custom-made heated surgical table, and was assessed with a rectal thermometer (Physitemp, Clifton, NJ, USA). Throughout the surgical preparation, end-tidal PCO_2 (P_{ETCO2}) was maintained at ~45 mmHg and monitored with a flow-through carbon dioxide analyzer designed to sufficiently measure response time for P_{ETCO2} measurements in rats (CapStar-100, CWE, Ardmore, PA).

Rats were bilaterally vagotomized and blood pressure was monitored in the right femoral artery by the insertion of a polyethylene catheter (PE50 ID: 0.58 mm, OD: 0.965 mm; Intramedic, MD, USA) connected to a pressure transducer (APT300 Pressure Transducer, Harvard Apparatus, Holliston, MA, USA). Arterial blood samples were taken during baseline, the first hypoxic episode, and at 15, 30 and at 60 min post-AIH and analyzed for partial pressures of O_2 (PO_2) and CO_2 (PCO_2) using a blood gas analyzer (ABL80 Flex, Radiometer, Brea, CA).

Through a dorsal approach, the left phrenic nerve was isolated, distally cut, desheathed, and covered with a saline soaked cotton ball until it was placed on a bipolar silver electrode

(described in the following section). Since isoflurane dampens phrenic nerve output, a minimum of 1 h was allowed following the conversion to urethane anesthesia before neurophysiological recordings began to eliminate this effect.

2.4. In vivo neurophysiological recordings

The left phrenic nerve was submerged in mineral oil and placed on bipolar silver electrodes to record nerve activity. Neural signals were amplified (10,000 ×), band-pass filtered (300–10,000 Hz, Model 1800, A-M Systems, Carlsborg, WA, USA), full-wave rectified, and integrated (50 ms time constant, MA-821, CWE Inc., Ardmore, PA, USA). Integrated nerve bursts were digitized (8 kHz) and analyzed using a WINDAQ data acquisition system (DATAQ Instruments, Akron, OH, USA). Apneic and recruitment thresholds were determined at least 1-h post urethane anesthesia conversion. First, ventilation was increased and P_{ETCO2} was reduced until rhythmic nerve bursts had ceased (i.e., apneic threshold). After 1 min of nerve cessation, the ventilator rate was decreased and P_{ETCO2} was slowly increased until the resumption of rhythmic nerve bursts occurred (i.e., recruitment threshold). To establish baseline conditions, P_{ETCO2} was held approximately 2 mmHg above the recruitment threshold until stabilization of neural activity had occurred (≥15 min). A baseline arterial blood sample was taken to document baseline blood gas levels. Following baseline measurements, rats were exposed to three 5-min episodes of isocapnic (±1.5 mmHg) acute intermittent hypoxia [10% inspired O_2, arterial PO_2 (PaO_2): 35–45 mmHg] separated by 5-min intervals of baseline O_2 conditions (50% inspired O_2, PaO_2: ≥150 mmHg). Rats were returned to baseline inspired O_2 levels after the third bout of hypoxia, and inspired O_2 levels were maintained for the duration of the experiments. Manipulation of inspired CO_2 and/or the ventilation rate was done to maintain isocapnic arterial PCO_2 ($PaCO_2$) within ±1.5 mmHg of the respective baseline value.

To test the hypothesis that COX-1/2 mediated inflammation plays a role in the differential pLTF observed in 7d and 28d CTB-SAP treated rats, rats were intraperitoneally (i.p.) injected with (*S*)-(+)-ketoprofen (keto; 12.5 mg/kg; Sigma-Aldrich, St. Louis, MO) or vehicle (veh; 50% ethanol and sterile saline; 100 μl/kg). 7d control treated groups included two groups that received AIH treatment: 1) keto ($n = 7$), and 2) keto veh ($n = 6$); and two groups that received no AIH treatment (time controls; TCs): 1) keto TC ($n = 3$), and 2) keto veh TC ($n = 4$). 28d control treated groups included two groups that received AIH treatment: 1) keto ($n = 7$), and 2) keto veh ($n = 5$); and two TC groups: 1) keto TC ($n = 4$), and 2) keto veh TC ($n = 4$). 7d CTB-SAP treated groups included two groups that received AIH treatment: 1) keto ($n = 6$), and 2) keto veh ($n = 6$); and two TC groups: 1) keto TC ($n = 3$), and 2) keto veh TC ($n = 3$). 28d CTB-SAP treated groups included two groups that received AIH treatment: 1) keto ($n = 8$), and 2) keto veh ($n = 5$); and two TC groups: 1) keto TC ($n = 4$), and 2) keto veh TC ($n = 3$). Since there were no apparent differences in TC groups (no AIH) and multiple previous studies demonstrating minimal experimental drift in time control experiments, all TC treated rats were grouped together per treatment (i.e., keto and keto veh) within control and CTB-SAP rats for statistical analyses. In this way, we were able to assure that keto and the vehicle did not elicit unexpected pMF (i. e. a time-dependent drift in time control experiments), while minimizing animal use consistent with national standards for animal research. Approximately 3 h after keto or keto veh delivery, animals

were exposed to either AIH or no AIH (TC), and phrenic nerve activity was recorded for 60 min after AIH or sham AIH.

2.5. Immunohistochemistry

Tissue used for staining was obtained from a separate set of rats than those used for the current neurophysiological studies that did not receive any drug or AIH treatment during neurophysiological experiments. Immediately following neurophysiological protocols, rats were transcardially perfused with cold 4% paraformaldehyde in phosphate buffered saline (0.01 M PBS, pH 7.4). Spinal cords were immediately removed following perfusion, post-fixed (4% paraformaldehyde in 0.01 M PBS) at 4 °C overnight, and then cryoprotected in graded sucrose (20% sucrose for 3 days and 30% sucrose for an additional 3 days) at 4 °C until sinking. The spinal cords were transversely sectioned (40 μm thick) using a freezing-sliding microtome (Leica SM 2000R, Germany), and stored at −20 °C in an antifreeze solution (30% glycerol, 30% ethylene glycol, 40% PBS). To evaluate microglial morphology in the phrenic motor nucleus of 7d and 28d control and CTB-SAP rats, six sections from C4 were selected for each animal ($n = 8$ per group).

Tissue was washed with 1× PBS three times for five minutes on a shaker at room temperature. Sections were then incubated at room temperature in a blocker solution (1× PBS + 0.2% Triton +5% normal donkey serum) on a shaker for 1 h. Sections were then incubated in primary antibody solution (1× PBS + 0.1% Triton +5% normal donkey serum + antibody against CTB (goat, 1:2000, Calbiochem) and Cd11b (mouse 1:500, Bio-Rad)) overnight at 4 °C on a shaker as conducted previously (Nichols et al., 2015). The following day, tissue was washed three times for 5 min at room temperature on a shaker in 1× PBS. The tissue was then incubated for 2 h at room temperature on a shaker in the dark in secondary antibody solution (1× PBS + 0.1% Triton +5% normal donkey serum + donkey anti-goat Alexa-Fluor 555 (1:1000; Molecular Probes, Eugene, OR) and donkey anti-mouse Alexa-Fluor 488 (1:1000; Molecular Probes, Eugene, OR)). Tissue was then washed again while covered in 1× PBS three times for 5 min on a shaker at room temperature. The tissue was then mounted on positively charged glass slides (Thermo Fisher Scientific, Waltham, MA) and allowed to dry before ProLong™ Gold anti-fade reagent (Thermo Fisher Scientific, Waltham, MA) was applied, and a coverslip was put onto the slides. Covered slides were stored at 4 °C until quantification of microglial morphology was performed.

2.6. Imaging

Photomicrographs were taken at the same settings for all images per antibody per group (i.e., gains for images: 555 (CTB) = 744.95, 488 (Cd11b) = 799.11). The photomicrographs were taken using a Leica DM4000 confocal microscope at 20× magnification with Leica Application Suite X (LAS X) software to encompass the CTB-labelled phrenic motor neurons in the C4 cervical spinal cord (Boulenguez et al., 2007; Mantilla et al., 2009; Nichols et al., 2015; Watson et al., 2009). Images were taken as 8-bit stacks at a resolution of 1024 × 1024 (366.67 μm × 366.67 μm).

2.7. Morphological analysis of microglia using IMARIS

Z stacks of all photomicrographs from all animals were opened in IMARIS software. The ROI set for the phrenic motor nucleus in the C4 sections was then used to create an ROI surface through the stack to incorporate 3D microglial projections. Once the high-resolution 3D surface was created, the CD11b + cells were masked to eliminate background pixilation in order to more appropriately trace microglial processes. Starting points were then placed in the cell body of each microglia within the ROI. Seed points were then placed along the projections and the software automatically created a skeleton of the projections so 3D morphological attributes could be quantified. Filament length sum (primary projections from cell body), branch length (secondary projections), branch volume sum, filament volume sum, number of branches, number of end-points, filament distance from the origin sum, and the number of microglia within the ROI were quantified as previously described (Cengiz et al., 2019). Quantification of each parameter was performed per microglia within the ROI. The parameters were then averaged across microglia within the ROI, and then averaged per animal and subsequently per group ($n = 8$ animals per group). A decrease in filament length sum, branch length, number of branches, number of end-points, filament distance from the origin, in addition to an increase in filament and branch volume would be indicative of amoeboid morphology. A Sholl analysis was also performed to quantify the branching density for each microglia within the ROI based on the number of intersections the branches make with a series of concentric circles (1 μm apart). From the Sholl analysis, the process maximum (N_m, the maximum number of intersections for the cell), and the critical value (Cr, the distance from the cell body where N_m occurred) per microglia were evaluated as previously described (Morrison and Filosa, 2013). These parameters were then averaged across microglia in the ROI, and then averaged per animal and subsequently per group. A decrease in the N_m and the Cr would be indicative of amoeboid morphology.

2.8. qRT-PCR for cervical spinal inflammatory-associated marker expression

Tissue used for qRT-PCR was obtained from a separate set of rats that did not undergo any prior studies. To begin to characterize the inflammatory response following CTB-SAP-induced respiratory motor neuron loss, cervical spinal (C3–5, which encompasses the phrenic motor nucleus) expression of inflammatory-associated markers was evaluated in control and CTB-SAP rats in the absence and presence of ketoprofen (12.5 mg/kg; IP delivery conducted 5 h prior to tissue collection). Rats were first perfused transcardially with 1× PBS, and the C3–5 spinal cord was isolated from each rat immediately after perfusion. Tissue homogenate samples were sonicated and resuspended in TRI-reagent (Invitrogen, Waltham, MA), which was followed by total RNA isolation according to the manufacturer's instructions. qRT-PCR was then used to determine TNF-α, BDNF, iNOS, and IL-10 gene expression since these markers have been shown to be implicated in the response to intermittent hypoxia and/or impact phrenic plasticity or breathing (Agosto-Marlin and Mitchell, 2017; Baertsch and Baker-Herman, 2015; Baker-Herman et al., 2004; Borkowski and Nichols, 2020; Broytman et al., 2013; Giannakopoulou et al., 2019; Huxtable et al., 2015). First, the RNA (1 μg) prepared from tissue samples of individual rats was reverse-transcribed into first-strand cDNA using an oligo(dT)/random hexamer cocktail and M-MLV Reverse Transcriptase (Invitrogen, Waltham, MA). The cDNA was then used for qRT-PCR using iTaq™ Universal SYBR® Green Supermix (BioRad Laboratories, Hercules,

CA), forward and reverse primers (primer sequences that were utilized are listed in Table 1), and DEPC water. Primer specificity was assessed through NCBI BLAST analysis prior to use, and all dissociation curves had a single peak with an observed melting temperature consistent with the intended amplicon sequences. Relative gene expression normalized to 18S was determined by the ΔΔCt method, and data was expressed as the fold change relative to controls in the absence or presence of ketoprofen. Sample size of treatment groups that did not receive ketoprofen: 7d control (TNF-α, BDNF, and IL-10, $n = 9$; iNOS, $n = 8$), 28d control ($n = 8$ for all genes), 7d CTB-SAP treated rats ($n = 7$ for all genes), and 28d CTB-SAP treated rats (TNF- α, BDNF, and IL-10, $n = 6$; iNOS, $n = 5$). Sample size of treatment groups that received ketoprofen: 7d control ($n = 7$ for all genes), 28d control (TNF-α, $n = 6$; BDNF, iNOS, and IL-10, $n = 7$), 7d CTB-SAP treated rats ($n = 10$ for all genes), and 28d CTB-SAP treated rats ($n = 10$ for all genes).

2.9. Statistical analysis

Integrated phrenic nerve burst amplitudes were averaged over 1 min during baseline and 15, 30, and 60 min after AIH. Peak integrated inspiratory phrenic nerve bursts at baseline were similar within treatment groups; thus nerve bursts were normalized to baseline measurements to appropriately quantify the magnitude of pLTF (expressed as a percentage change from baseline). Statistical comparisons between treatment groups for AIH studies (amplitude, $PaCO_2$, PaO_2, and mean arterial pressure) were done using a two-way ANOVA with a repeated-measures design. Since there were no differences between successive hypoxic exposure within groups ($p > 0.05$, data not shown), comparisons of the short-term hypoxic phrenic response were made using a one-way ANOVA, in which phrenic burst amplitude during the fifth minute of hypoxic episodes was averaged from all three episodes. For TC rats receiving no AIH exposure, a two-way ANOVA with repeated-measures design was performed; since there were no differences among them, they were grouped into single TC groups per treatment (i.e., keto and keto veh) within control and CTB-SAP rats (keto veh TC control, $n = 8$; keto veh TC CTB-SAP, $n = 6$; keto TC control, $n = 7$; keto TC CTB-SAP, $n = 7$). A one-way ANOVA was used when comparing phrenic nerve burst amplitudes across groups at 60 min post-hypoxia, and when comparing the qRT-PCR data across groups where 7d and 28d controls were combined into one control group since no differences were detected between time points in the absence (TNF-α, BDNF, and IL-10, $n = 17$; iNOS, $n = 16$) or presence of ketoprofen (TNF-α, $n = 13$; BDNF, iNOS, and IL-10, $n = 14$). For parameters evaluated using IMARIS software in the phrenic motor nucleus, the 7d and 28d control and CTB-SAP rats were grouped together in their respective treatment groups because no differences were observed between time points within each treatment. A *t*-test was then performed to compare control rats to CTB-SAP rats. When significant ANOVA differences were detected, individual comparisons were made with Fisher's least significant difference post hoc test (Sigma Plot version 14.0; Systat Software Inc., San Jose, CA, USA). Differences between the groups were considered significant if $p < 0.05$; all values are expressed as means ± S.E.M.

3. Results

3.1. Blood gases and mean arterial pressures

Despite small but significant differences within and across groups for arterial PCO_2 ($PaCO_2$), $PaCO_2$ was successfully maintained within 1.5 mmHg from its baseline value in all groups (Table 2). Therefore, changes in integrated phrenic nerve burst amplitude following AIH is not attributed to differences in chemoreceptor feedback (changes >1.5 mmHg of baseline in $PaCO_2$ can influence pLTF; Bach and Mitchell, 1996). For AIH, arterial PaO_2 (PaO_2) was successfully regulated within the target range (35–45 mmHg), and remained above 150 mmHg at all time points post-hypoxia (Table 2). As expected, mean arterial pressure differed among groups when AIH vs. TCs were compared during hypoxic episodes, and slight but significant differences within groups were < 20 mmHg at 60 mins post-hypoxia, and this was consistent among groups [Table 2; changes in mean arterial pressure of <20 mmHg from baseline values have minimal effect on respiratory activity in rats (Walker and Jennings, 1996; Bach and Mitchell, 1996)]. Thus, the differential pLTF expression observed was not affected by differences in $PaCO_2$, PaO_2, or blood pressure regulation.

3.2. Short-term hypoxic phrenic responses

Since phrenic responses were not different across hypoxic episodes within AIH treated groups ($p > 0.05$; data not shown), responses during the three episodes were combined in each rat and then compared across treatment groups (Fig. 1). Time control (TC) groups were not exposed to AIH, and did not exhibit a significant change in amplitude during the sham AIH exposure as expected (Fig. 1; $p > 0.05$). All AIH-treated groups had hypoxic responses that were significantly increased vs. corresponding TC groups (Fig. 1; $p < 0.05$). Although all AIH groups elicited significant phrenic nerve hypoxic responses, 7d CTB-SAP rats pre-treated with keto veh had a greater phrenic nerve hypoxic response vs. all other treatment groups exposed to AIH, regardless of time point and pre-treatment (Fig. 1; $p < 0.05$).

3.3. Ketoprofen delivery hinders pLTF at 7d, while it enhances pLTF in 28d CTB-SAP treated rats

One purpose of the current study was to understand if COX-1/2 mediated inflammation plays a role in the differential pLTF observed in CTB-SAP treated rats. Representative phrenic neurograms are shown for AIH-exposed 7d and 28d CTB-SAP rats approximately 3 h following keto veh or keto (Figs. 2A,B and 3A,B). As expected, all groups exposed to AIH elicited pLTF that was significantly greater than baseline and corresponding TCs at 60 min (Figs. 2C,D, 3C,D and 4; $p < 0.05$). However, when 7d CTB-SAP rats were pre-treated with keto, pLTF was attenuated from that of 7d CTB-SAP rats pre-treated with keto veh ($p < 0.05$), and appeared similar to 7d control rats that received AIH regardless of pre-treatment (Figs. 2C,D and 4; $p > 0.05$). In contrast, AIH-induced pLTF was enhanced when 28d CTB-SAP rats were pretreated with keto compared to 28d CTB-SAP rats pre-treated with keto veh and 28d controls treated with keto or keto veh (Figs. 3C,D and 4; $p < 0.05$). Interestingly, the enhanced pLTF observed in 28d CTB-SAP rats pre-treated with keto was similar to that of 7d CTB-SAP rats pre-treated with keto veh (Fig. 4; $p > 0.05$). Together,

these data indicate that COX-1/2 mediated inflammation contributes to the enhanced pLTF observed in 7d CTB-SAP rats, and is constraining pLTF in 28d CTB-SAP rats.

3.4. Microglial morphological changes are exhibited in the phrenic motor nucleus of CTB-SAP rats

Neuroinflammation is mediated primarily through glial cells (e.g., astrocytes, oligodendrocytes, and microglia). Microglia are the resident immune cells of the CNS that react to injury by undergoing phenotypic changes that are affiliated with pro- and anti-inflammatory states both molecularly and morphologically. Here, we evaluated morphological changes in microglia within the phrenic motor nucleus of CTB-SAP rats vs. controls using IMARIS software. Consistent with our previous findings (Nichols et al., 2015), microglial number was increased in CTB-SAP rats compared to controls (Table 3 and Fig. 5). IMARIS software was also used to evaluate parameters that are indicative of ramified or amoeboid morphological states. The software was used to three-dimensionally mask immunopositive Cd11b pixels on the microglia within the phrenic motor nucleus (Fig. 5A and B). Through an automated process performed by IMARIS software, starting points were then placed on the soma of the microglia and seed points were placed along the projections of the microglia (Fig. 5C and D). The microglia were then cast into a 3D object in which filament and branching parameters were calculated from the starting point. Significant decreases in filament length sum (μm), filament distance from the origin sum (μm), and number of intersections were observed in CTB-SAP rats compared to controls ($p < 0.05$; Table 3). This would suggest that the microglia in the phrenic motor nucleus in CTB-SAP rats are more amoeboid-like in morphological state. However, we did not observe significant differences in other parameters that were studied including branch length, branch number, branch volume sum, filament volume sum, number of end points, and intersection distance ($p > 0.05$; Table 3).

3.5. Cervical spinal inflammatory-associated marker expression in CTB-SAP rats

Cervical spinal (C3–5, which encompasses the phrenic motor nucleus) inflammatory-associated marker expression was evaluated using qRT-PCR in control rats and in rats following CTB-SAP-induced respiratory motor neuron loss in the absence and presence of ketoprofen. qRT-PCR was performed on homogenate C3–5 samples to quantify fold changes in CTB-SAP rats relative to controls +/− ketoprofen for the following inflammatory-associated markers: TNF-α, BDNF, iNOS, and IL-10. Significant increases were observed in the absence of ketoprofen for TNF-α (7d and 28d), BDNF (28d only), and IL-10 (28d only) expression in CTB-SAP rats vs. controls ($p < 0.05$; Fig. 6A). iNOS expression was not significantly different between groups in the absence of ketoprofen ($p > 0.05$; Fig. 6A). In the presence of ketoprofen, a significant increase was observed for BDNF expression in 7d CTB-SAP rats vs. control and 28d CTB-SAP rats ($p < 0.05$; Fig. 6B), while the expression of all other C3–5 inflammatory-associated markers was not different between groups [i.e., TNF-α (7d and 28d), BDNF (28d), and IL-10 (28d) expression was decreased back to control levels in the presence of ketoprofen].

4. Discussion

Here, we demonstrate that pLTF following CTB-SAP induced respiratory motor neuron loss at 7d and 28d is differentially affected following ketoprofen delivery, and that expression of cervical spinal (C3–5) inflammatory-associated markers is increased in CTB-SAP rats which can be reversed with ketoprofen delivery. When bilateral intrapleural injections of CTB-SAP (25 μg) are given, respiratory motor neurons die, but eupnea is maintained (Nichols et al., 2018; Nichols et al., 2015). AIH-induced pLTF has been shown to be enhanced in 7d CTB-SAP rats compared to control rats and 28d CTB-SAP rats (Nichols et al., 2018), and it has been shown that 7d CTB-SAP rats predominately utilize the Gs pathway for pLTF whereas 28d CTB-SAP rats utilize the Gq pathway (Borkowski and Nichols, 2020; Borkowski et al., 2021). This enhancement is no longer observed at 7d in CTB-SAP rats pre-treated with ketoprofen (Figs. 2D and 4). Conversely, pre-treatment with ketoprofen enhanced pLTF in 28d CTB-SAP treated rats (Figs. 3D and 4). In addition, we see changes in microglial expression and morphology at these different time points (Fig. 5 and Table 3), indicating they may play a role in the differences in the AIH-induced pLTF observed at 7d and 28d. The major findings of this study include: 1) COX-1/2 signaling contributes to the enhanced AIH-induced pLTF observed in 7d CTB-SAP rats; 2) COX-1/2 signaling constrains AIH-induced pLTF in 28d CTB-SAP rats; 3) microglia are morphologically amoeboid-like in the phrenic motor nucleus of CTB-SAP rats; and 4) C3–5 inflammatory-associated marker expression (TNF-α, BDNF, and IL-10) is increased in CTB-SAP rats, and ketoprofen delivery decreases this expression back to control levels.

4.1. COX-1/2 signaling contributes to enhanced pLTF in 7d CTB-SAP rats, while it constrains pLTF in 28d CTB-SAP rats

Our findings in the current study suggest that initiation of the enhanced pLTF observed in 7d CTB-SAP rats is mediated in part by the activation of cyclooxygenase-1 and -2 (COX-1 and COX-2) enzymes. When 7d CTB-SAP rats were pre-treated with the nonsteroidal COX-1/2 inhibitor, ketoprofen, AIH-induced pLTF was no longer enhanced and appeared similar to that of control rats pre-treated with keto veh (Figs. 2-4). Conversely, when 28d CTB-SAP rats were pre-treated with ketoprofen, AIH-induced pLTF was enhanced to that of 7d CTB-SAP rats pre-treated with keto veh (Figs. 3 and 4). Consistent with prior studies, ketoprofen did not have an effect on pLTF in control rats (Huxtable et al., 2013). The results in the current study show that COX-1/2 signaling contributes to the enhanced pLTF in 7d CTB-SAP rats, but constrains pLTF exhibited by 28d CTB-SAP rats.

The mechanism(s) by which COX mediated inflammation impacts pLTF following CTB-SAP-induced respiratory motor death at 7d and 28d remains unknown. However, since CTB-SAP intrapleural injections results in cell death through apoptotic mechanisms induced by saporin, we speculate that NF-κB (nuclear factor kappa-light-chain-enhancer of activated B cells) and MAPK-mediated transcriptional signaling (Hanamsagar et al., 2012) is increased in dying respiratory motor neurons, which then upregulates COX-2 expression and stimulates the release of circulating pro-inflammatory cytokines such as tumor necrosis factor alpha (TNF-α; Fig. 6) and interleukin-1 beta (IL-1β) (Kreutzberg, 1996). IL-1 and TNF-α receptors are located on neurons, microglia, and astrocytes (Lampron et al., 2013;

Probert, 2015) indicating that inflammatory stimulation can be sensed and evoked between multiple cell types, as well as within cell types of the same phenotype. Our data demonstrate that cervical spinal TNF-α expression is increased in the absence of ketoprofen and is then reversed back to control levels in the presence of ketoprofen in 7d CTB-SAP rats (Fig. 6), which suggests that TNF-α contributes to inflammation-resistant pLTF at this time point since pLTF is attenuated following ketoprofen treatment (Figs. 2 and 4). Previous studies have shown that TNF-α signaling in the spinal cord affects spinal plasticity by increasing the trafficking of AMPA receptors to the post-synaptic membrane leading to an up-regulation of Ca^{2+} permeable Glutamate receptor 2 (GluR2)-lacking AMPA receptors that ultimately increases postsynaptic excitability (Beattie et al., 2002). TNF-α activity has also been shown to be sufficient for pMF and is required for a form of respiratory plasticity that results from reduction in central respiratory neural activity, known as inactivity-induced phrenic motor facilitation (iPMF) (Baertsch and Baker-Herman, 2013; Baertsch and Baker-Herman, 2015; Baker-Herman and Strey, 2011; Broytman et al., 2013; Mahamed et al., 2011). Therefore, it is possible that TNF-α production alone can elicit plasticity in our model of CTB-SAP-induced respiratory motor neuron loss (which may explain why we no longer see pLTF enhancement in 7d CTB-SAP rats with COX-1/2 inhibition since we may be interfering with TNF-α signaling), and we speculate that CTB-SAP rats may also exhibit TNF-α dependent iPMF. However, the requirement of TNF-α for phrenic plasticity in 7d CTB-SAP rats remains unknown.

Furthermore, inflammation can diminish pLTF in a variety of ways, one being through IL-1 receptor activation (Hocker and Huxtable, 2018). Although we did not measure IL-1β expression in this study, we speculate that an initial increase in IL-1β in 7d CTB-SAP rats could be leading to increased p38 MAPK signaling. This signaling may increase glutamate release to the postsynaptic neuron (Kotlyarov et al., 1999) and contribute to the enhanced pLTF observed in 7d CTB-SAP rats. This same signaling pathway has been shown to be vital in the abolishment of Gq-dependent pLTF following sustained intermittent hypoxia (Huxtable et al., 2015); therefore, this may be another way 7d CTB-SAP rats (which utilize the Gs pathway for pLTF) are resistant to inflammation-induced pLTF depression.

Additionally, we observe that TNF-α, BDNF, and IL-10 expression is increased in 28d CTB-SAP rats in the absence of ketoprofen, and are all reversed back to control levels in the presence of ketoprofen (Fig. 6). When studied in the context of hypoxia, TLR4 expression was increased on microglia through HIF-1α (hypoxia-inducible factor 1α), which then led to the release of pro-inflammatory mediators through the NF-κB pathway (Hanamsagar et al., 2012; Yao et al., 2013). Although the mechanism is unknown, the expression of TNF-α has been shown to be dependent on hypoxia-induced COX-2 activation (Xing et al., 2015). Additionally, BDNF transcription is positively regulated by TNF-α in astroglia (Saha et al., 2006). Therefore, we speculate that the increase we observe in TNF-α expression is contributing to the simultaneous increase in BDNF expression which results in a magnitude of pLTF that is similar to controls (*i.e.,* not enhanced as we observe in 7d CTB-SAP rats) in the absence of ketoprofen in 28d CTB-SAP rats, and would be consistent with prior studies demonstrating that 28d CTB-SAP rats exhibit BDNF-dependent pLTF (Borkowski and Nichols, 2020). Furthermore, we posit that the reversal of TNF-α and BDNF expression back to control levels allows the constraint on pLTF to be released in the presence of

ketoprofen in 28d CTB-SAP rats. In addition, suppression of BDNF has been shown to be beneficial when studied in spinal cord injury since BDNF suppression limited astrocyte proliferation and prevented astrogliosis (Tu et al., 2017). Thus, it may be possible that abnormal astrocyte proliferation and cytokine production is constraining pLTF in 28d CTB-SAP rats, and this is alleviated through the inhibition of COX-2 and subsequent reduction in TNF-α dependent BDNF overproduction. This same pattern between TNF-α and BDNF expression, however, is not observed in 7d CTB-SAP rats. Interestingly, even though we see a significant increase in TNF-α expression in the absence of ketoprofen in 7d CTB-SAP rats that is then reduced to control levels by ketoprofen pre-treatment (Fig. 6), we do not see an increase in BDNF expression from controls without ketoprofen intervention (Fig. 6A). A significant increase in BDNF expression is only observed once ketoprofen is administered in 7d CTB-SAP rats vs. controls and 28d CTB-SAP rats (Fig. 6B). Therefore, we speculate that astrocyte activation leads to astrocyte proliferation through increased BDNF signaling, which may contribute to constraining pLTF following COX-1/2 inhibition in 7d CTB-SAP rats. However, the role of BDNF expression and whether it constrains pLTF in the presence of ketoprofen in 7d CTB-SAP rats remains unknown and will be tested in future studies.

Furthermore, expression of IL-10 receptors has been described in various respiratory-related areas, including on microglia, and has been shown to be involved with regulating breathing (Geerling et al., 2010; Giannakopoulou et al., 2019; Jiang et al., 2013). Thus, we speculate that IL-10 may be involved in the regulation of pLTF in 28d CTB-SAP rats. However, it remains unknown if inhibition of TNF-α, BDNF, and/or IL-10 expression are required for the enhanced pLTF we observe in the presence of ketoprofen and whether this is beneficial in 28d CTB-SAP rats. Future studies will focus on microglial and astrocyte cytokine release and the interactions these cytokines have with the differential mechanisms of pLTF utilized by 7d and 28d CTB-SAP rats.

4.2. Microglial morphology is impacted in CTB-SAP treated rats

Under normal conditions, microglia are considered to be in a resting state, but are continually surveying the environment with ramified branching (Parkhurst and Gan, 2010; Raivich, 2005). Upon injury, microglia migrate to the site of injury and begin to undergo morphological changes that can be pro-inflammatory or anti-inflammatory. The number of microglia in the phrenic motor nucleus was significantly increased in CTB-SAP rats compared to controls when evaluated with IMARIS software (Table 3 and Fig. 5), which is consistent with our previous study (Nichols et al., 2015). When we evaluated microglial morphological parameters using IMARIS software in the phrenic motor nucleus, we found that CTB-SAP rats had decreased primary branching and a smaller number of branch intersections using the Sholl analysis (Table 3 and Fig. 5), which is indicative of a more amoeboid-like morphological state compared to the microglia observed in controls.

Lastly, in vitro research has shown that serotonin and ATP facilitate microglial migration (Krabbe et al., 2012). Thus, it is possible that CTB-SAP-induced respiratory motor neuron death could lead to the release of ATP and signal microglial migration to respiratory motor nuclei. However, microglia are not the only cell types involved in neuro-inflammation. Astrocytes should also be evaluated for their density, morphology, and molecular changes in

CTB-SAP rats, since astrocytes are increased in neurodegenerative disease models following respiratory motor neuron loss (Howland et al., 2002).

4.3. Significance

Since inflammation differentially affects AIH-induced pLTF at different time points following respiratory motor neuron death, future directions will be focused on understanding which underlying pro- and anti-inflammatory factors are produced by microglia in these motor nuclei in CTB-SAP treated rats. Our data provide insight into time-dependent cytokine expression which may explain the differences in the pLTF response to ketoprofen over the course of motor neuron loss in CTB-SAP rats. Thus, future studies will focus on determining whether these factors impact pLTF and breathing (e.g., contribute vs. constrain). Inflammatory responses (and associated cell types) following respiratory motor neuron death must be investigated further to better understand when and what type of intervention would be beneficial to improve breathing following respiratory motor neuron loss. Furthermore, by understanding differences in the mechanisms involved and the impact of inflammation on respiratory plasticity and breathing, we can more accurately treat patients with nonsteroidal drugs throughout varying stages of respiratory motor neuron loss.

Acknowledgments

The authors thank Safraaz Mahammed for the custom-designed computer program used for in vivo neurophysiology data analysis, and the Dalton Cardiovascular Research Center Imaging Core Facilities for the use of the confocal microscope. Additionally, the authors would like to thank Dr. Doug Bowles for laboratory access and use of the Bio-Rad IQ5 Multi-color Real-Time PCR system, and Dr. Darla Tharp for her insight and expertise in operating the equipment.

Abbreviations:

BDNF	brain-derived neurotrophic factor
CTB	cholera toxin B
CTB-SAP	cholera toxin B conjugated to saporin
COX-1/2	cyclooxygenase-1/2
IL-10	interleukin 10
keto	ketoprofen
P_{ETCO2}	partial pressure of end-tidal carbon dioxide
$PaCO_2$	partial pressure of arterial carbon dioxide
PaO_2	partial pressure of arterial oxygen
pLTF	phrenic long-term facilitation
TNF-α	tumor necrosis factor alpha

References

Agosto-Marlin IM, Mitchell GS, 2017. Spinal BDNF-induced phrenic motor facilitation requires PKCθ activity. J. Neurophysiol 118, 2755–2762. [PubMed: 28855298]

Agosto-Marlin IM, Nichols NL, Mitchell GS, 2018. Systemic inflammation inhibits serotonin receptor 2-induced phrenic motor facilitation upstream from BDNF/TrkB signaling. J. Neurophysiol 119, 2176–2185. [PubMed: 29513151]

Bach KB, Mitchell GS, 1996. Hypoxia-induced long-term facilitation of respiratory activity is serotonin dependent. Respir. Physiol 104, 251–260. [PubMed: 8893371]

Baertsch NA, Baker-Herman TL, 2013. Inactivity-induced phrenic and hypoglossal motor facilitation are differentially expressed following intermittent vs. sustained neural apnea. J. Appl. Physiol 114, 1388–1395. [PubMed: 23493368]

Baertsch NA, Baker-Herman TL, 2015. Intermittent reductions in respiratory neural activity elicit spinal TNF-alpha-independent, atypical PKC-dependent inactivity-induced phrenic motor facilitation. Am. J. Phys. Regul. Integr. Comp. Phys 308, R700–R707.

Baker-Herman TL, Strey KA, 2011. Similarities and differences in mechanisms of phrenic and hypoglossal motor facilitation. Respir. Physiol. Neurobiol 179, 48–56. [PubMed: 21745601]

Baker-Herman TL, Fuller DD, Bavis RW, Zabka AG, Golder FJ, Doperalski NJ, Johnson RA, Watters JJ, Mitchell GS, 2004. BDNF is necessary and sufficient for spinal respiratory plasticity following intermittent hypoxia. Nat. Neurosci 7, 48–55. [PubMed: 14699417]

Beattie EC, Stellwagen D, Morishita W, Bresnahan JC, Ha BK, Von Zastrow M, Beattie MS, Malenka RC, 2002. Control of synaptic strength by glial TNFα. Science 295, 2282–2285. [PubMed: 11910117]

Boentert M, Wenninger S, Sansone VA, 2017. Respiratory involvement in neuromuscular disorders. Curr. Opin. Neurol 30, 529–537. [PubMed: 28562381]

Borkowski LF, Nichols NL, 2020. Differential mechanisms are required for phrenic long-term facilitation over the course of motor neuron loss following CTB-SAP intrapleural injections. Exp. Neurol 113460. [PubMed: 32916172]

Borkowski LF, Smith CL, Keilholz AN, Nichols NL, 2021. Divergent receptor utilization is necessary for phrenic long-term facilitation over the course of motor neuron loss following CTB-SAP intrapleural injections. J. Neurophysiol 126, 709–722. [PubMed: 34288779]

Boulenguez P, Gestreau C, Vinit S, Stamegna J-C, Kastner A, Gauthier P, 2007. Specific and artifactual labeling in the rat spinal cord and medulla after injection of monosynaptic retrograde tracers into the diaphragm. Neurosci. Lett 417, 206–211. [PubMed: 17412505]

Bourke S, Shaw P, Gibson G, 2001. Respiratory function vs sleep-disordered breathing as predictors of QOL in ALS. Neurology 57, 2040–2044. [PubMed: 11739823]

Broytman O, Baertsch NA, Baker-Herman TL, 2013. Spinal TNFα is necessary for inactivity-induced phrenic motor facilitation. J. Physiol 591, 5585–5598. [PubMed: 23878370]

Cengiz P, Zafer D, Chandrashekhar JH, Chanana V, Bogost J, Waldman A, Novak B, Kintner DB, Ferrazzano PA, 2019. Developmental differences in microglia morphology and gene expression during normal brain development and in response to hypoxia-ischemia. Neurochem. Int 127, 137–147. [PubMed: 30639264]

Devinney MJ, Huxtable AG, Nichols NL, Mitchell GS, 2013. Hypoxia-induced phrenic long-term facilitation: emergent properties. Ann. N. Y. Acad. Sci 1279, 143–153. [PubMed: 23531012]

Devinney MJ, Fields DP, Huxtable AG, Peterson TJ, Dale EA, Mitchell GS, 2015. Phrenic long-term facilitation requires PKCθ activity within phrenic motor neurons. J. Neurosci 35, 8107–8117. [PubMed: 26019328]

Geerling JC, Shin JW, Chimenti PC, Loewy AD, 2010. Paraventricular hypothalamic nucleus: axonal projections to the brainstem. J. Comp. Neurol 518, 1460–1499. [PubMed: 20187136]

Giannakopoulou CE, Sotiriou A, Dettoraki M, Yang M, Perlikos F, Toumpanakis D, Prezerakos G, Koutsourelakis I, Kastis GA, Vassilakopoulou V, Mizi E, Papalois A, Greer JJ, Vassilakopoulos T, 2019. Regulation of breathing pattern by IL-10. Am. J. Phys. Regul. Integr. Comp. Phys 317, R190–R202.

Golder FJ, Ranganathan L, Satriotomo I, Hoffman M, Lovett-Barr MR, Watters JJ, Baker-Herman TL, Mitchell GS, 2008. Spinal adenosine A2a receptor activation elicits long-lasting phrenic motor facilitation. J. Neurosci 28, 2033–2042. [PubMed: 18305238]

Graeber MB, 2010. Changing face of microglia. Science 330, 783–788. [PubMed: 21051630]

Hanamsagar R, Hanke ML, Kielian T, 2012. Toll-like receptor (TLR) and inflammasome actions in the central nervous system. Trends Immunol. 33, 333–342. [PubMed: 22521509]

Hocker AD, Huxtable AG, 2018. IL-1 receptor activation undermines respiratory motor plasticity after systemic inflammation. J. Appl. Physiol 125, 504–512. [PubMed: 29565772]

Hocker AD, Stokes JA, Powell FL, Huxtable AG, 2017. The impact of inflammation on respiratory plasticity. Exp. Neurol 287, 243–253. [PubMed: 27476100]

Hoffman MS, Nichols NL, MacFarlane PM, Mitchell GS, 2012. Phrenic long-term facilitation after acute intermittent hypoxia requires spinal ERK activation but not TrkB synthesis. J. Appl. Physiol 113, 1184–1193. [PubMed: 22961271]

Howland DS, Liu J, She Y, Goad B, Maragakis NJ, Kim B, Erickson J, Kulik J, DeVito L, Psaltis G, 2002. Focal loss of the glutamate transporter EAAT2 in a transgenic rat model of SOD1 mutant-mediated amyotrophic lateral sclerosis (ALS). Proc. Natl. Acad. Sci 99, 1604–1609. [PubMed: 11818550]

Huston JM, Tracey KJ, 2011. The pulse of inflammation: heart rate variability, the cholinergic anti-inflammatory pathway and implications for therapy. J. Intern. Med 269, 45–53. [PubMed: 21158977]

Huxtable A, Vinit S, Windelborn J, Crader S, Guenther C, Watters J, Mitchell G, 2011. Systemic inflammation impairs respiratory chemoreflexes and plasticity. Respir. Physiol. Neurobiol 178, 482–489. [PubMed: 21729770]

Huxtable AG, Smith SM, Vinit S, Watters JJ, Mitchell GS, 2013. Systemic LPS induces spinal inflammatory gene expression and impairs phrenic long-term facilitation following acute intermittent hypoxia. J. Appl. Physiol 114, 879–887. [PubMed: 23329821]

Huxtable AG, Smith SM, Peterson TJ, Watters JJ, Mitchell GS, 2015. Intermittent hypoxia-induced spinal inflammation impairs respiratory motor plasticity by a spinal p38 MAP kinase-dependent mechanism. J. Neurosci 35, 6871–6880. [PubMed: 25926462]

Jiang N, Shi P, Desland F, Kitchen-Pareja MC, Sumners C, 2013. Interleukin-10 inhibits angiotensin II-induced decrease in neuronal potassium current. Am. J. Phys. Cell Physiol 304, C801–C807.

Kotlyarov A, Neininger A, Schubert C, Eckert R, Birchmeier C, Volk H-D, Gaestel M, 1999. MAPKAP kinase 2 is essential for LPS-induced TNF-α biosynthesis. Nat. Cell Biol 1, 94–97. [PubMed: 10559880]

Krabbe G, Matyash V, Pannasch U, Mamer L, Boddeke HW, Kettenmann H, 2012. Activation of serotonin receptors promotes microglial injury-induced motility but attenuates phagocytic activity. Brain Behav. Immun 26, 419–428. [PubMed: 22198120]

Kreutzberg GW, 1996. Microglia: a sensor for pathological events in the CNS. Trends Neurosci. 19, 312–318. [PubMed: 8843599]

Lampron A, ElAli A, Rivest S, 2013. Innate immunity in the CNS: redefining the relationship between the CNS and its environment. Neuron 78, 214–232. [PubMed: 23622060]

Lechtzin N, Wiener CM, Shade DM, Clawson L, Diette GB, 2002. Spirometry in the supine position improves the detection of diaphragmatic weakness in patients with amyotrophic lateral sclerosis. Chest 121, 436–442. [PubMed: 11834654]

Lu Y-C, Yeh W-C, Ohashi PS, 2008. LPS/TLR4 signal transduction pathway. Cytokine 42, 145–151. [PubMed: 18304834]

Lyall R, Donaldson N, Polkey M, Leigh P, Moxham J, 2001. Respiratory muscle strength and ventilatory failure in amyotrophic lateral sclerosis. Brain 124, 2000–2013. [PubMed: 11571218]

Mahamed S, Strey KA, Mitchell GS, Baker-Herman TL, 2011. Reduced respiratory neural activity elicits phrenic motor facilitation. Respir. Physiol. Neurobiol 175, 303–309. [PubMed: 21167322]

Mantilla CB, Zhan W-Z, Sieck GC, 2009. Retrograde labeling of phrenic motoneurons by intrapleural injection. J. Neurosci. Methods 182, 244–249. [PubMed: 19559048]

Mitchell GS, Baker TL, Nanda SA, Fuller DD, Zabka AG, Hodgeman BA, Bavis RW, Mack KJ, Olson E Jr., 2001. Invited review: intermittent hypoxia and respiratory plasticity. J. Appl. Physiol 90, 2466–2475. [PubMed: 11356815]

Morrison HW, Filosa JA, 2013. A quantitative spatiotemporal analysis of microglia morphology during ischemic stroke and reperfusion. J. Neuroinflammation 10, 4. [PubMed: 23311642]

Nichols NL, Dale EA, Mitchell GS, 2012. Severe acute intermittent hypoxia elicits phrenic long-term facilitation by a novel adenosine-dependent mechanism. J. Appl. Physiol 112, 1678–1688. [PubMed: 22403346]

Nichols NL, Van Dyke J, Nashold L, Satriotomo I, Suzuki M, Mitchell G, 2013. Ventilatory control in ALS. Respir. Physiol. Neurobiol 189, 429–437. [PubMed: 23692930]

Nichols NL, Vinit S, Bauernschmidt L, Mitchell GS, 2015. Respiratory function after selective respiratory motor neuron death from intrapleural CTB–saporin injections. Exp. Neurol 267, 18–29. [PubMed: 25476493]

Nichols NL, Craig TA, Tanner MA, 2018. Phrenic long-term facilitation following intrapleural CTB-SAP-induced respiratory motor neuron death. Respir. Physiol. Neurobiol 256, 43–49. [PubMed: 28822818]

Nogués MA, Roncoroni AJ, Benarroch E, 2002. Breathing control in neurological diseases. Clin. Auton. Res 12, 440–449. [PubMed: 12598948]

Parkhurst CN, Gan W-B, 2010. Microglia dynamics and function in the CNS. Curr. Opin. Neurobiol 20, 595–600. [PubMed: 20705452]

Perry VH, 2010. Contribution of systemic inflammation to chronic neurodegeneration. Acta Neuropathol. 120, 277–286. [PubMed: 20644946]

Probert L, 2015. TNF and its receptors in the CNS: the essential, the desirable and the deleterious effects. Neuroscience 302, 2–22. [PubMed: 26117714]

Raivich G, 2005. Like cops on the beat: the active role of resting microglia. Trends Neurosci. 28, 571–573. [PubMed: 16165228]

Saha RN, Liu X, Pahan K, 2006. Up-regulation of BDNF in astrocytes by TNF-α: a case for the neuroprotective role of cytokine. J. NeuroImmune Pharmacol. 1, 212–222. [PubMed: 18040799]

Teeling J, Perry V, 2009. Systemic infection and inflammation in acute CNS injury and chronic neurodegeneration: underlying mechanisms. Neuroscience 158, 1062–1073. [PubMed: 18706982]

Triantafilou M, Triantafilou K, 2002. Lipopolysaccharide recognition: CD14, TLRs and the LPS-activation cluster. Trends Immunol. 23, 301–304. [PubMed: 12072369]

Tu Z, Li Y, Dai Y, Li L, Lv G, Chen I, Wang B, 2017. MiR-140/BDNF axis regulates normal human astrocyte proliferation and LPS-induced IL-6 and TNF-α secretion. Biomed. Pharmacother 91, 899–905. [PubMed: 28501777]

Vinit S, Windelborn JA, Mitchell GS, 2011. Lipopolysaccharide attenuates phrenic long-term facilitation following acute intermittent hypoxia. Respir. Physiol. Neurobiol 176, 130–135. [PubMed: 21334467]

Walker JK, Jennings DB, 1996. Ventilatory effects of angiotensin and vasopressin in conscious rats. Can. J. Physiol. Pharmacol 74, 1258–1264. [PubMed: 9028585]

Watson C, Paxinos G, Kayalioglu G, 2009. The Spinal Cord: A Christopher and Dana Reeve Foundation Text and Atlas. Academic Press.

Wong PC, Cai H, Borchelt DR, Price DL, 2002. Genetically engineered mouse models of neurodegenerative diseases. Nat. Neurosci 5, 633–639. [PubMed: 12085093]

Xing Y, Wang R, Chen D, Mao J, Shi R, Wu Z, Kang J, Tian W, Zhang C, 2015. COX2 is involved in hypoxia-induced TNF-α expression in osteoblast. Sci. Rep 5, 1–7.

Yao L, Kan EM, Lu J, Hao A, Dheen ST, Kaur C, Ling E-A, 2013. Toll-like receptor 4 mediates microglial activation and production of inflammatory mediators in neonatal rat brain following hypoxia: role of TLR4 in hypoxic microglia. J. Neuroinflammation 10, 1–21. [PubMed: 23282009]

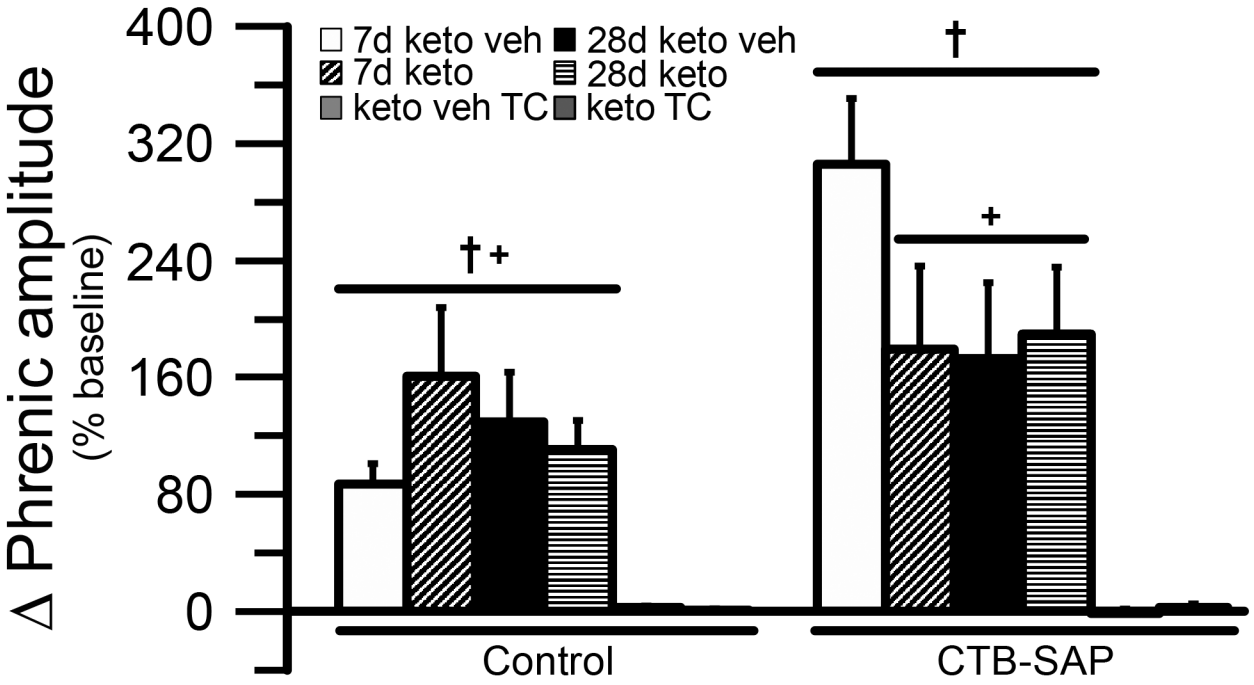

Fig. 1.

Short-term phrenic nerve hypoxic response in 7d & 28d control and CTB SAP treated rats. Short-term phrenic nerve hypoxic responses were compared in 7d and 28d control and CTB-SAP treated rats pre-treated with ketoprofen (keto) or keto vehicle (keto veh). As expected, all treatment groups exposed to AIH had a significantly greater hypoxic response vs. the corresponding time control (TC) groups (†). 7d CTB-SAP rats pre-treated with keto veh had a greater phrenic nerve hypoxic response vs. all other treatment groups exposed to AIH (+). Values are expressed as means ±1 S.E.M, and differences were considered significant if $p < 0.05$.

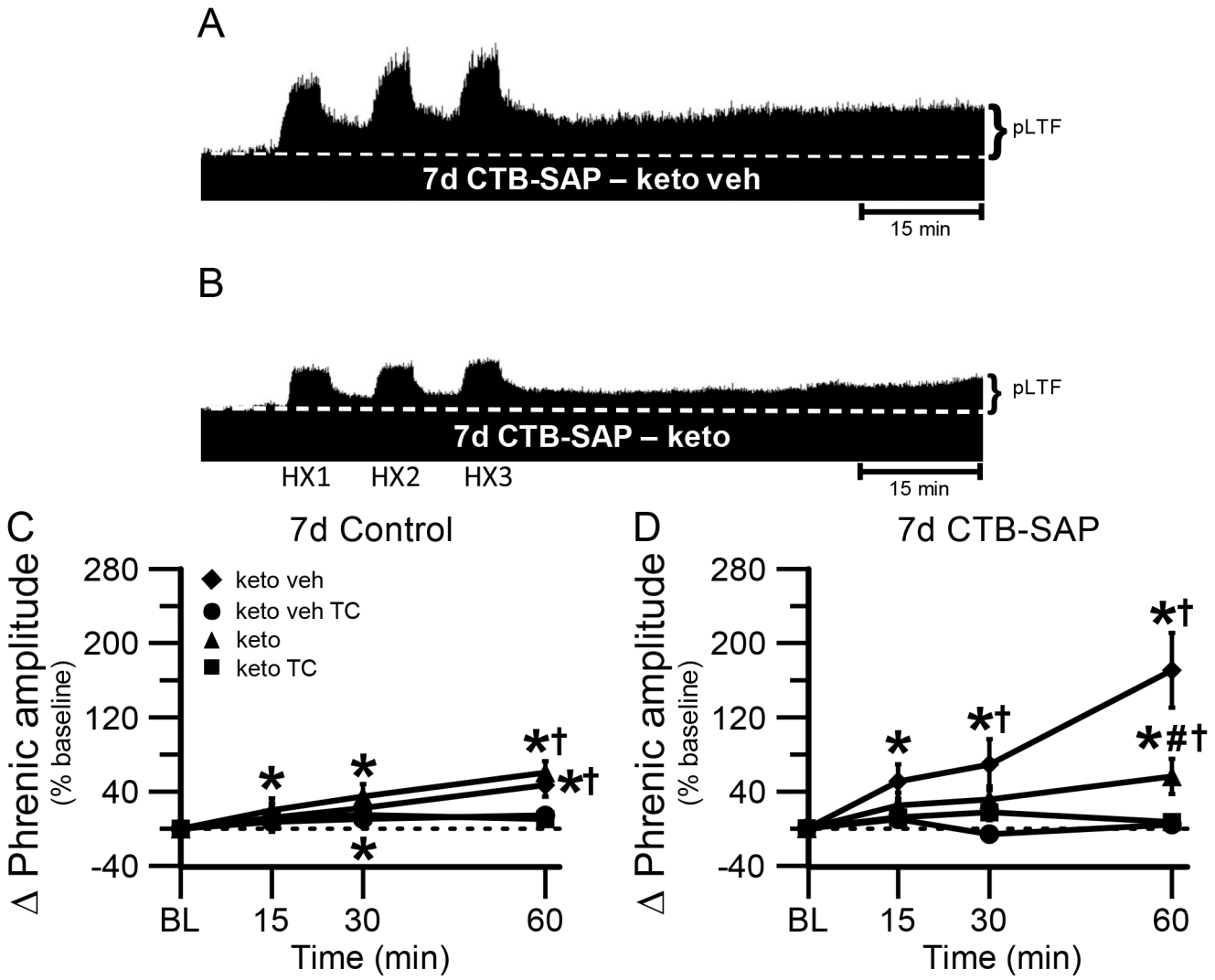

Fig. 2.

pLTF in 7d treated rats. A and B, Representative traces of compressed, integrated phrenic nerve activity before and after AIH in 7d CTB-SAP rats pre-treated with keto veh (A) or keto (B). Baseline is indicated in each trace by a white, dashed line. AIH elicits an enhanced pLTF in 7d CTB-SAP rats pre-treated with keto veh, while pLTF appears to be more moderate with keto pre-treatment. C, D. Phrenic burst amplitude (expressed as a percent change from baseline) in 7d control (C) and 7d CTB-SAP (D) rats pre-treated with keto veh, keto veh TC, keto, or keto TC. pLTF was significantly increased from baseline (*) at all time points in 7d control rats pretreated with keto and at 30 and 60 min post-hypoxia in those pre-treated with keto veh. pLTF was significantly increased from respective TCs at 60 min (†) in 7d control (C) and CTB-SAP (D) rats pre-treated with keto or keto veh. pLTF was significantly increased from baseline (*) at all time points in 7d CTB-SAP rats pre-treated with keto veh and at 60 min for those pre-treated with keto. 7d CTB-SAP rats pre-treated with keto had a pLTF that was significantly less than that of 7d CTB-SAP rats

pre-treated with keto veh (#). Values are expressed as means ±1 S.E. M, and differences were considered significant if $p < 0.05$.

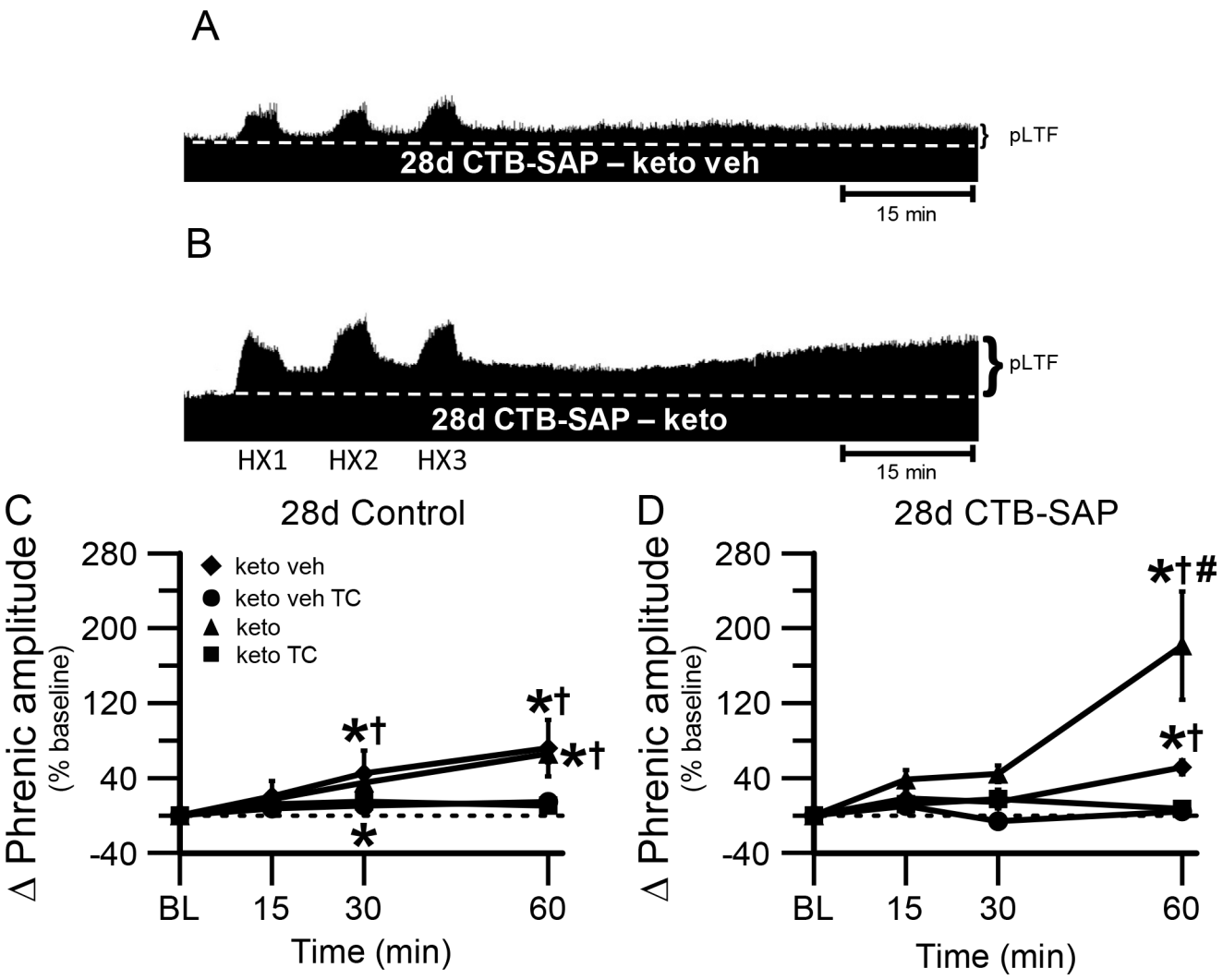

Fig. 3.

pLTF in 28d treated rats. A and B, Representative traces of compressed, integrated phrenic nerve activity before and after AIH in 28d CTB-SAP rats pre-treated with keto veh (A) or keto (B). Baseline is indicated in each trace by a white, dashed line. AIH elicits an enhanced pLTF in 28d CTB-SAP rats pre-treated with keto, while pLTF appears to be more moderate with keto veh pre-treatment. C, D. Phrenic burst amplitude (expressed as a percent change from baseline) in 28d control (C) and 28d CTB-SAP (D) rats pre-treated with keto veh, keto veh TC, keto, or keto TC. pLTF was significantly increased from baseline (*) at 30 and 60 min in 28d control rats pre-treated with keto veh and keto, and 60 min in 28d CTB-SAP rats with the same pre-treatments. pLTF was significantly greater than respective time controls at 30 and 60 min in 28d control rats pre-treated with keto veh, and at 60 min in 28d control and CTB-SAP rats pre-treated with keto and 28d CTB-SAP rats pre-treated with keto veh (†). 28d CTB-SAP rats pre-treated with keto had a significantly greater pLTF than that of 28d CTB-SAP rats pre-treated with keto veh (#). Values are expressed as means ±1 S.E.M, and differences were considered significant if $p < 0.05$.

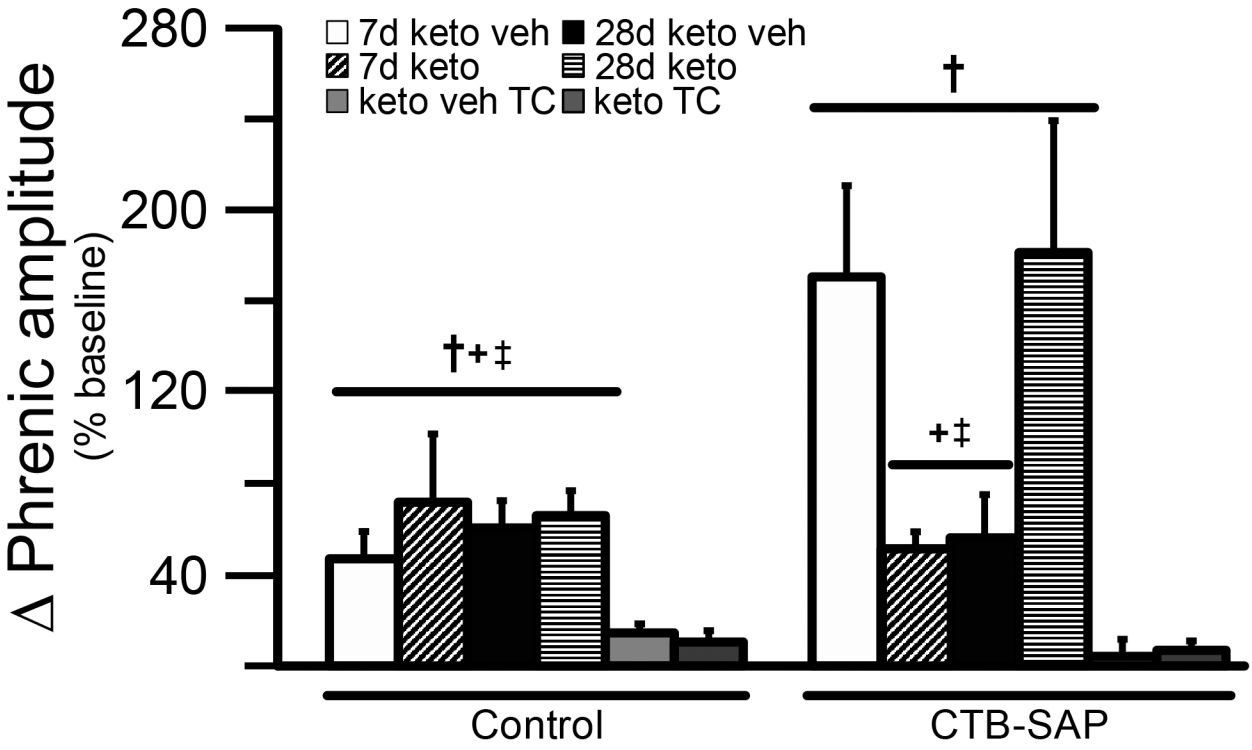

Fig. 4.

Direct comparisons of the change in phrenic amplitude (percent baseline) following AIH at 60 min post-hypoxia in 7d & 28d control and CTB-SAP treated rats. pLTF was compared in 7d and 28d control and CTB-SAP treated rats pre-treated with keto veh, keto, keto veh TC, or keto TC. 7d and 28d control and CTB-SAP rats exhibited greater pLTF vs. the corresponding TC groups (†). 7d CTB-SAP rats pre-treated with keto veh and 28d CTB-SAP rats pre-treated with keto had a pLTF that was significantly greater than all control groups, 28d CTB-SAP rats pre-treated with keto veh, and 7d CTB-SAP rats pre-treated with keto (+ and ‡, respectively). Values are expressed as means ±1 S.E.M, and differences were considered significant if $p < 0.05$.

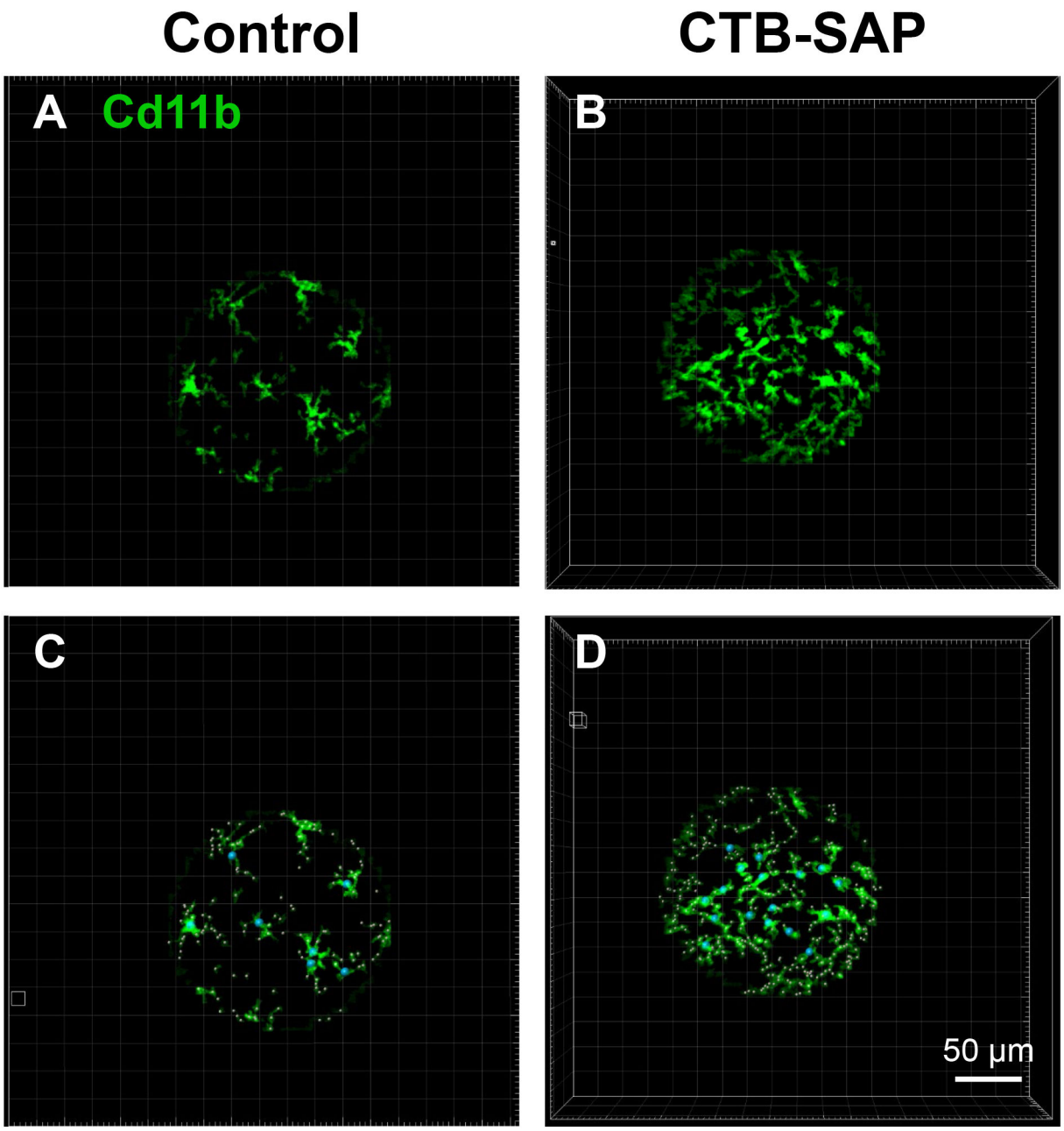

Fig. 5.

IMARIS analysis of microglial morphology in the phrenic motor nucleus in control and CTB-SAP rats. A-D. Representative images of Cd11b (green) labelled microglia within the phrenic motor nucleus from C4 cervical spinal cord segments from a control (A and C) and CTB-SAP (B and D) rat. Note, there appears to be an increase in the number of microglia within the phrenic motor nucleus of the CTB-SAP rat as represented by the increase in green (B) vs. the control (A) rat. C and D. Images were masked to eliminate staining that was artifact, and starting points (blue circles) were inserted on the soma of the microglia. Seed points (pink small circles) were then inserted along the projections, and the

IMARIS software then calculated various parameters related to filament and branch length and volume. The closer the seed points are to the starting point, the shorter the projections are from the soma of the microglia, which is indicative of an amoeboid morphological state as depicted in CTB-SAP rats (B and D). (For interpretation of the references to color in this figure legend, the reader is referred to the web version of this article.)

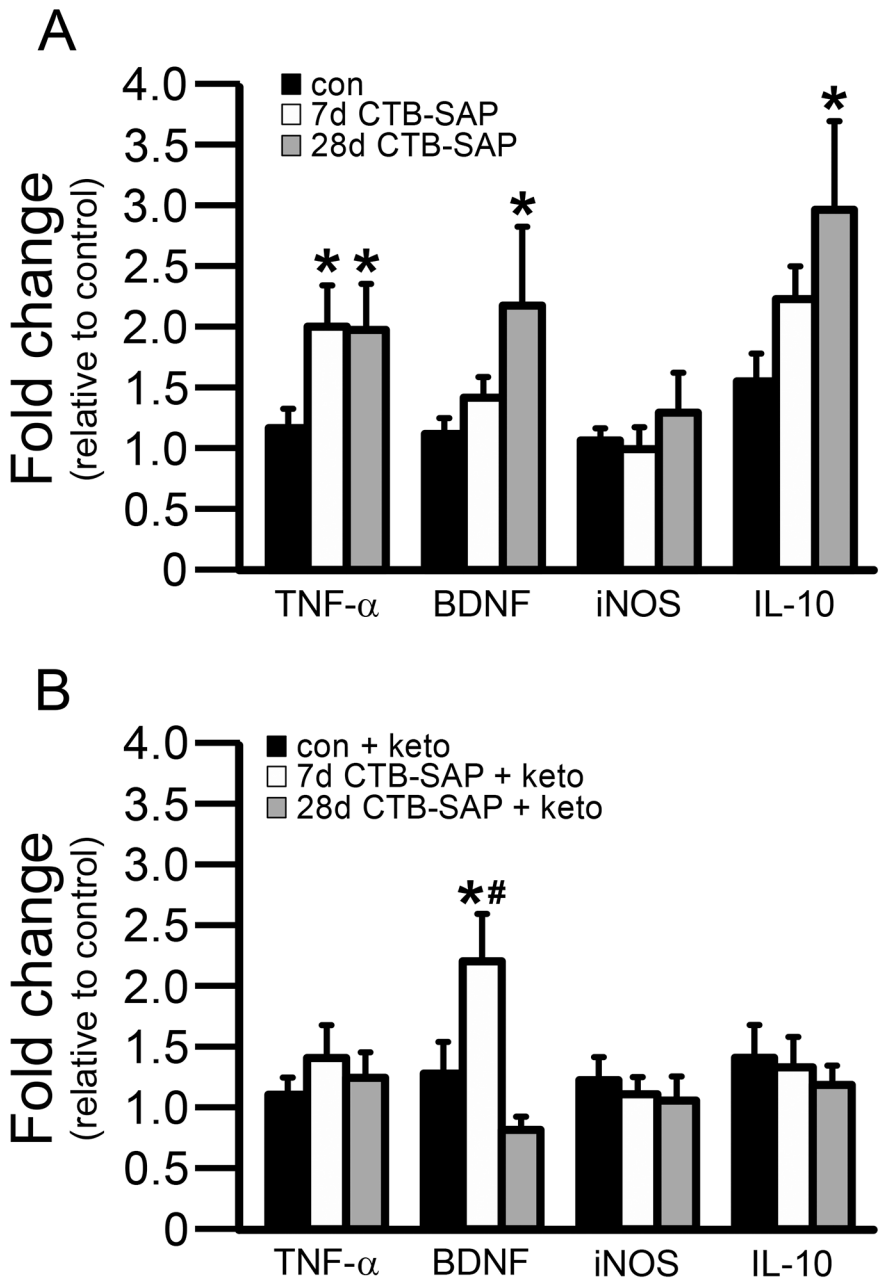

Fig. 6.

Cervical spinal (C3–5) inflammatory-associated marker expression in control and CTB-SAP rats. Pro- and anti-inflammatory cytokine expression was evaluated in homogenate cervical spinal cord (C3–5) tissue encompassing the phrenic motor nucleus in the absence (A) and presence (B) of ketoprofen. TNF-α (7d and 28d), BDNF (28d only), and IL-10 (28d only) expression is increased in CTB-SAP rats vs. controls in the absence of ketoprofen (*). In the presence of ketoprofen, only BDNF expression was increased in 7d CTB-SAP rats vs. controls (*) and 28d CTB-SAP rats (#). Values are expressed as means ±1 S.E.M, and differences were considered significant if $p < 0.05$.

Table 1:

Primer sequences for qRT-PCR analyses.

Gene Name	Forward sequence (5')	Reverse sequence (5')
18s	CGGGTGCTCTTAGCTGAGTGTCCCG	CTCGGGCCTGCTTTGAACAC
TNF-α	TGCCACTTCATACCAGGAGA	CCGGAGTCCGTGATGTCTA
BDNF	CCCATCACAATCTCACGGTAATC	TGCGGAGGGTCTCCTATGAA
iNOS	AGGGAGTGTTGTTCCAGGTG	TCTGCAGGATGTCTTGAACG
IL-10	AAGTGATGCCCCAGGCAGAGAA	AAATCGATGACAGCGTCGCAGC

Table 2:

Arterial PCO_2, PO_2 and mean arterial pressure (MAP) during baseline, hypoxia (HX) and 60 minutes post-hypoxia for control and CTB-SAP treated rats with acute intermittent hypoxia (AIH) or without AIH (time-control or TC). Rats received ketoprofen (keto) or keto vehicle (veh) delivery (IP). Significant differences within groups included *versus* hypoxia ([a]), and 60 min ([b]), and across groups included *versus*: respective TC ([c]), keto veh 28d CON ([d]), keto 28d CTB-SAP ([e]), keto 7d CTB-SAP ([f]), keto 7d CON ([g]), and keto veh 7d CON ([h]). Values are expressed as means ± 1 S.E.M. Differences were considered significant if $p<0.05$.

	P_{aCO2} (mmHg)			P_{aO2} (mmHg)			MAP (mmHg)		
Experimental Groups	**baseline**	**hypoxia**	**60 min**	**baseline**	**hypoxia**	**60 min**	**baseline**	**hypoxia**	**60 min**
With AIH Keto veh									
7d CON	46.9±1.2	47.2±0.9	46.9±1.1	287±7[ab]	42.2±1.2[c]	258±16[a]	118±6	97±16	117±17
7d CTB-SAP	49.6±1.3	49.3±1.1	49.5±1.4	312±6[abcf]	39.8±1.3[c]	270±11[a]	108±5	85±8	101±8
28d CON	46.1±0.7[b]	45.9±0.6	47.4±0.4[a]	314±12[af]	42.8±1.2[c]	297±11[a]	106±7	87±11	98±6
28d CTB-SAP	46.7±1.7	46.4±1.7[e]	47.1±1.3	311±5[acf]	38.8±2.7[c]	288±13[a]	123±8[a]	80±16	108±6[a]
Keto									
7d CON	46.8±1.2	47.1±1.3	47.4±0.9	290±5[a]	40.9±2.0[c]	270±13[a]	104±6[a]	73±9[c]	124±21[a]
7d CTB-SAP	49.3±2.0[b]	48.3±1.3	50.7±1.4[a]	268±30[a]	36.0±1.9[c]	247±31[ad]	106±4[a]	80±5	92±17[g]
28d CON	47.9±1.0	48.5±1.2	48.3±1.5	306±10[a]	39.4±0.6[c]	295±13[af]	106±12	91±7[c]	86±12[gh]
28d CTB-SAP	50.1±1.1[d]	50.4±0.9[d]	50.7±1.0	316±4[abcf]	40.6±1.8[c]	280±11[a]	109±6[a]	75±6[c]	92±6[gh]
Without AIH (TCs)									
CON keto veh	49.4±1.6	49.3±1.8	49.7±1.7	290±13	293±11	279±7	108±3	108±5	105±4
CTB-SAP keto veh	49.2±0.8	49.8±1.0	49.3±1.1	254±18	271±11	279±11	108±6	109±6	110±6
CON keto	50.3±1.6[d]	50.2±1.7[d]	50.5±1.4	306±6	304±7	287±7	123±3	120±5	107±9
CTB-SAP keto	49.4±1.5	49.6±1.5	49.1±1.4	256±27	264±28	260±20	125±13	105±7	105±5

Rats received ketoprofen (keto) or keto vehicle (veh) delivery (IP). Significant differences within groups included versus hypoxia (a), and 60 min (b), and across groups included versus: respective TC (c), keto veh 28d CON (d), keto 28d CTB-SAP (e), keto 7d CTB-SAP (f), keto 7d CON (g), and keto veh 7d CON (h). Values are expressed as means ± 1 S.E.M. Differences were considered significant if $p<0.05$.

Table 3.

Morphology of microglia within the phrenic motor nucleus in control and CTB-SAP rats. Morphological parameters were averaged for each group, and compared between control and CTB-SAP treated rats. Significant decreases were observed for filament length sum (μm), filament distance from the origin sum (μm), and the max number of intersections in CTB-SAP rats *vs.* controls, while the number of microglia was significantly increased in CTB-SAP rats *vs.* controls ([a]). Values are expressed as means ± 1 S.E.M. Differences were considered significant if $p<0.05$.

Parameters	Control	CTB-SAP
Branch length (μm)	7.94 ± 0.11	7.90 ± 0.07
Branch number	5.44 ± 0.33	4.59 ± 0.32
Branch volume sum (μm^3)	50.2 ± 1.17	52.3 ± 1.03
Filament length sum (μm)	104 ± 4.50	89.1 ± 5.08[a]
Filament volume sum (μm^3)	656 ± 29.6	587 ± 35.8
Filament distance from the origin sum (μm)	273 ± 3.15	264 ± 2.81[a]
Number of end-points	7.96 ± 0.38	6.88 ± 0.40
Number of microglia	7.33 ± 0.66	14.2 ± 1.29[a]
Number of intersections	5.83 ± 0.18	5.06 ± 0.18[a]
Intersection distance (μm)	7.91 ± 0.24	7.51 ± 0.26

Morphological parameters were averaged for each group, and compared between control and CTB-SAP treated rats. Significant decreases were observed for filament length sum (μm), filament distance from the origin sum (μm), and the max number of intersections in CTB-SAP rats vs. controls, while the number of microglia was significantly increased in CTB-SAP rats vs. controls (a). Values are expressed as means ± 1 S.E.M. Differences were considered significant if $p<0.05$.